Material and design engineering of (Al)GaN for high-performance avalanche photodiodes and intersubband applications

M. Razeghi* and C. Bayram
Center for Quantum Devices; Department of Electrical Engineering and Computer Science;
Northwestern University; Evanston, Illinois 60208; USA

ABSTRACT

Numerous applications in scientific, medical, and military areas demand robust, compact, sensitive, and fast ultraviolet (UV) detection. Our (Al)GaN photodiodes pose high avalanche gain and single-photon detection efficiency that can measure up to these requirements. Inherit advantage of back-illumination in our devices offers an easier integration and layout packaging via flip-chip hybridization for UV focal plane arrays that may find uses from space applications to hostile-agent detection. Thanks to the recent (Al)GaN material optimization, III-Nitrides, known to have fast carrier dynamics and short relaxation times, are employed in (Al)GaN based superlattices that absorb in near-infrared regime. In this work, we explain the origins of our high performance UV APDs, and employ our (Al)GaN material knowledge for intersubband applications. We also discuss the extension of this material engineering into the far infrared, and even the terahertz (THz) region.

Keywords: avalanche gain, ultraviolet, AlGaN, superlattice, intersubband absorption, terahertz

1. INTRODUCTION

1.1 III-Nitride Avalanche Photodiodes

Wide bandgap III-nitride semiconductors have been the subject of intense scientific and technological developments since the 1990's, primarily driven by the quest for blue lasers and high brightness visible light emitting diodes.[1,2] In parallel, III-nitrides have also been studied extensively for use in ultraviolet (UV) photodetectors due to their potential to offer intrinsic visible- or solar-blind detection, which is highly desirable for a number of applications.[3] Using a visible- or solar-blind detector eliminates the need for expensive and efficiency-limiting optical filters to remove undesired out-of-band visible or solar photons. This makes them well suited for numerous applications in the defense, commercial, and scientific arenas including covert space-to-space communications, early missile threat detection, chemical and biological threat detection and spectroscopy, flame detection and monitoring, UV environmental monitoring, and UV astronomy. [1,3]

However, despite the apparent advantages of III-Nitride based photodetectors, many of these applications are still dominated by the use of photomultiplier tubes (PMT). PMTs are capable of obtaining very high sensitivity using internal electron multiplication gain (typically ~10^6); with proper choice of the photocathode material it is also possible to obtain a degree of visible- or solar-blindness. However these detectors are not without their drawbacks: they are bulky, fragile glass tubes that require large biases (typically 1000 V) to operate effectively.[4] Therefore, it is highly desirable to develop a compact semiconductor-based photodetector capable of realizing this level of sensitivity.[5, 6] In principle this can be obtained in III-Nitrides by taking advantage of avalanche multiplication under high electric fields – typically 2.7 MV/cm, which with proper design can correspond to an external reverse bias of less than 100 volts.[7]

Despite the relative ease of growing front-illuminated GaN APDs, the realization of back-illuminated GaN APDs has been demonstrated to be more advantageous.[8] A back-illuminated *p-i-n* GaN structure, in which photons reach the *n*-type layer first, results in primarily the injection of holes into the high-gain multiplication region. This results in higher gain and better overall performance since, near the critical field strength, the hole impact ionization coefficient is higher than the electron impact ionization coefficient in GaN.[9] We have experimentally confirmed this and extracted experimental values for the impact ionization coefficient for holes and electrons in GaN by designing a device that can be operated under either front- or back-illumination, thereby injecting either primarily holes or primarily electrons.[8] In addition, the integration of APD arrays with read-out electronics becomes easier.

* razeghi@eecs.northwestern.edu; phone 1 (847) 491-7251; fax 1 (847) 476-1817; http://cqd.eecs.northwestern.edu

Photonic Materials, Devices, and Applications III, edited by Ali Serpengüzel, Gonçal Badenes, Giancarlo C. Righini,
Proc. of SPIE Vol. 7366, 73661F · © 2009 SPIE · CCC code: 0277-786X/09/$18 · doi: 10.1117/12.819390

The use of separate absorption and multiplication (SAM) regions in avalanche photodiodes is a common approach to reduce multiplication noise and enhance gain through impact-ionization engineering.[10, 11] We present the design, fabrication, and characterization of GaN avalanche photodiodes with a separate absorption and multiplication design allowing for nearly pure injection of holes into the multiplication region, offering lower noise performance and higher gain, benefiting from the higher ionization coefficient for holes. It is also crucial to carefully control the material quality and the doping. The breakdown voltage of APDs is largely determined by the electric field build up in the device, and the voltage at which the critical electric field is reached. Because the dark current tends to increase with voltage, reducing the breakdown voltage can be advantageous in achieving higher gains. For a given multiplication width, the primarily limitation on the electric field build up is the low carrier concentration of the *p*-GaN layer. The *p*-GaN quality is low due to (1) trade-offs in growth conditions since those at which Mg incorporation is maximized may degrade GaN quality; and (2) the high activation energy of Mg requires that the Mg incorporation in the lattice be almost 100 times higher than the desired carrier concentration leading to a disruption of the GaN lattice.[12] In order to overcome this we have investigated the use of a novel δ-doping technique for the realization of high-quality *p*-GaN.[13] Compared to regular bulk *p*-type doping, δ-doped *p*-GaN layers have been shown to have higher structural and electrical quality. By incorporating δ-doped *p*-GaN into a SAM-APD structure we present devices with superior performance.[7]

1.2 III-Nitride Intersubband Devices

III-Nitrides are promising candidates for intersubband devices due to their inherently fast carrier dynamics and short relaxation times. However, realizing high quality material for intersubband devices presents a significant challenge. The tunibility of the layer thicknesses and control of the material quality is essential for intersubband absorption. Molecular beam epitaxy (MBE) has been preferred for AlN/GaN superlattices as interfaces and layer thicknesses could be monitored in-situ more conveniently than with metalorganic chemical vapor deposition (MOCVD). However, it is known that III-Nitrides with high Al compositions can be grown with much higher quality by MOCVD due to greater flexibility in the growth conditions (such as growth in higher temperatures). Thus, MOCVD could be the key for future ISB devices based on III-Nitrides.

III-nitride room temperature intersubband luminescence at ~2 μm has been demonstrated.[14] However, for the far-infrared and THz regimes, only theoretical estimates are available. The feasibility of laser action in GaN/AlGaN cascade structure is indicated.[15] Room temperature lasing by optical pumping at 34 μm[16] suggests more experimental work should be carried out in this field to realize compact high power semiconductor based THz emitters. Intersubband (ISB) transitions have shown quite a lot of potential for optoelectronics in the mid- and far-infrared spectral regions. One promising application is ISB quantum cascade lasers that will find many applications. In the near infrared spectral region, optical communication as well as chemical/biological sensing are key applications. Recently, various reported ISB absorption in near-infrared (1.1-1.6 μm) in GaN/Al(Ga)N superlattices.[17,18,19,20,21] Although there are many reports of ISB absorption at telecommunications wavelengths (1.3 -1.55 μm) for MBE-grown materials[17,18,20], there are few reports for MOCVD grown material[19] and fewer leading to absorption lower than 2 μm. [22] Our first aim is to succeed ISB transition in mid-infrared to reach in a second step the THz range by decreasing the energy difference between the two states involved.[23], [24]

2. APD MATERIAL GROWTH AND PROCESSING

2.1 APD Template Growth

The material was grown in a commercial AIXTRON 200/4-HT horizontal flow low-pressure metalorganic chemical vapor deposition (MOCVD) reactor. In order to allow for back-illumination of the device double-side polished (00.1) sapphire was used as the substrate. Growth on the sapphire substrate was nucleated with a thin 200 Å low-temperature AlN buffer layer. On top of this a 600 nm thick high quality AlN template layer was grown by atomic layer epitaxy at a temperature of ~1300°C. This template layer is crucial to realizing high performance back illuminated devices: it allows the active region to be displaced from the highly defected low temperature buffer layer while being completely transparent to wavelengths longer than 210 nm. Atomic force microscopy of the surface of this template shows a well ordered surface with uniform atomic steps clearly visible and a sub-angstrom RMS roughness. This layer has an open-detector (00.2) X-ray full-width half-maximum of 41 arc-seconds owing to the excellent crystalline quality of the material.[6]

2.2 APD Device Structures

On top of this high quality AlN template layer, the GaN epilayers that make up the device are grown at 100 mBar using hydrogen as the precursor gas. This GaN growth is accomplished without the use of an intermediate buffer layer. The GaN layer surface is very smooth (~1.3 Å RMS roughness) with very few observable dislocation termination pits. The active region of the device consists of either a GaN *p-i-n* or *p-i-n-i-n* homojunction based structure. The *p*-type GaN:Mg layer has a hole concentration of ~1×10^{18} cm^{-3}, and it either grown via conventional growth or via δ-doping; the intrinsic GaN multiplication and/or absorption regions have a residual concentration of ~2.5×10^{16} cm^{-3}; and, the intentionally doped *n*-type GaN:Si layer has a electron concentration of ~2×10^{18} cm^{-3}. A schematic of a conventional APD device structure is shown on the left of Figure 1. The right of Figure 1 shows the SAM-APD structure.

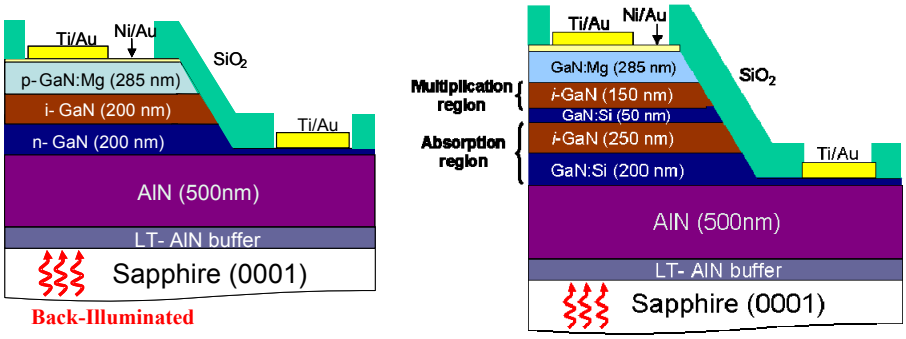

Figure 1. Left) a conventional *p-i-n* APD structure. Right) the separate absorption and multiplication device structure. The GaN:Mg in either structure can be grown either conventionally or via δ-doping.

2.3 Device Processing

All samples are first annealed at 1000 ºC for 30 seconds under dry N_2 for magnesium activation of the either conventionally grown or δ-doping grown *p*-type GaN:Mg layer. The material is then patterned into arrays of circular and square detectors with areas ranging from 225 μm^2 up to 14,063 μm^2 using electron cyclotron resonance (ECR-RF) dry etching to reach the bottom *n*-type GaN:Si contact layer. A thin 30 Å Ni / 30 Å Au layer was then deposited on top of the mesas and annealed under ambient air at 500 ºC for 10 minutes in order to form ohmic contact to the *p*-type GaN. A 400 Å Ti / 1200 Å Au metal layer was deposited on the GaN:Si layer to form the common *n*-type contact and on top of the thin Ni/Au as a thick metal contact to aid in contacting the device. The devices are finally covered with 300 nm of SiO_2 deposited by plasma enhance chemical vapor deposition to help protect the mesas and prevent premature breakdown of the devices; windows are opened via wet etching.

3. SEPARATE ABSORBTION AND MULTIPLICATION AVALANCE PHOTODIODES

The SAM-APD uses a *p-i-n-i-n* structure as shown on the right of Figure 1. Based upon this structure and the doping described in the growth section, the electric field profile can be calculated from a one-dimensional finite element model. This is shown below on the right of Figure 2 with electric field of a reference structure shown on the left for comparison purposes. At low voltages, the electric field is mainly localized in the topmost *i*-GaN layer (multiplication region). The increase of the reverse bias enhances the electric field in this layer and broadens the depletion region towards the *p*-GaN and across the *n*-GaN layer towards the other *i*-GaN layer. This intrinsic layer becomes fully depleted at the reach-through voltage (V_{rt} = 40 V).

3.1 Photon Absorption in SAM-APDs

Absorption measurements performed on reference samples gave a band edge absorption coefficient of ~1×10^{5} cm^{-1}. From this value it is possible to calculate the absorption profile of the entire structure when illuminated from the back (assuming no contribution from the sapphire or AlN, or any reflection losses). This is done for both the conventional APD structure and the SAM-APD structure, and plotted below in Figure 2. In the conventional APD structure approximately 75% of the photons are absorbed in the *n*-GaN region, with the remaining 25% being absorbed directly in the intrinsic multiplication region. The exact ratio depends on the electric field, becoming worse at higher electric field strengths. In the SAM-APD structure light absorption in the bottom *n*-GaN and *i*-GaN layers combined account for 99%

of the absorption. This results in nearly pure hole-injection into the multiplication region. However, the absorption properties change for photon energies above or below the bandgap[25]: as the photon energy increases above the bandgap, the light becomes mainly absorbed in the bottom *n*-GaN, closer to the AlN interface; contrarily, as the energy decreases below the bandgap, the light becomes mainly absorbed in the upper layers.[26] In particular, the Franz-Keldysh effect may raise the absorption coefficient in the multiplication region at longer wavelengths.[27]

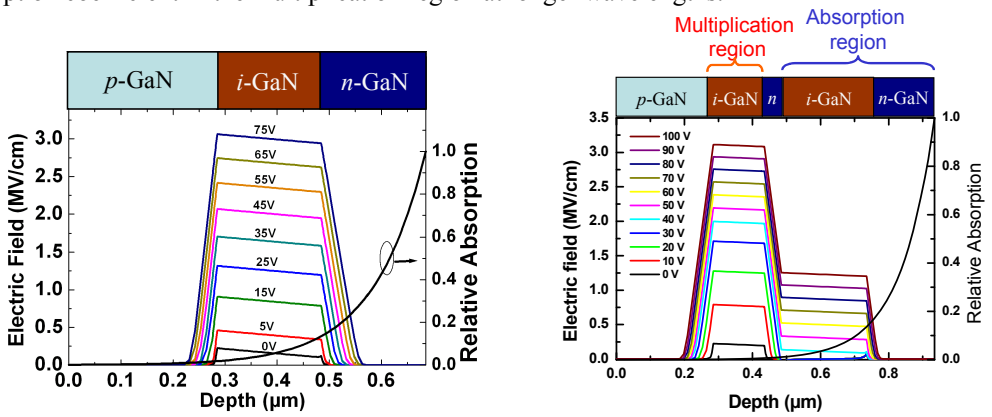

Figure 2. Left) Electric field profile and relative photon absorption profile of a conventional *p*-*i*-*n* APD showing absorption in both the *n*-GaN and *i*-GaN layers. Right) Electric field profile and relative photon absorption profile of a SAM-APD showing most of the absorption taking place before photons reach the multiplication region.

3.2 Performance of SAM-APDs

The current-voltage (*I*-*V*) characteristics under reverse bias were measured in darkness and under illumination, using the Xe lamp filtered at 360 nm (optical power = 4.1 nW). The light and dark *I*-*V* curves were measured alternatively three times in a row to ensure statistically meaningful and consistent device operation. The data is plotted below in Figure 3; the error bars on this figure indicate the standard deviation of the measurements. In darkness, the current remains below the measurement limit up to 30 V. Beyond that voltage, dark current increases monotonously until reaching the breakdown voltage at 95 V, at which point the device exhibits a dark current of 10 nA. At this voltage, the electric field profile predicts an average value of about 3 MV/cm in the multiplication region, in fairly good agreement with the value of the critical electric field in GaN.[8] A sharp increase of the dark current is observed above breakdown reaching 70 μA at 111 V.

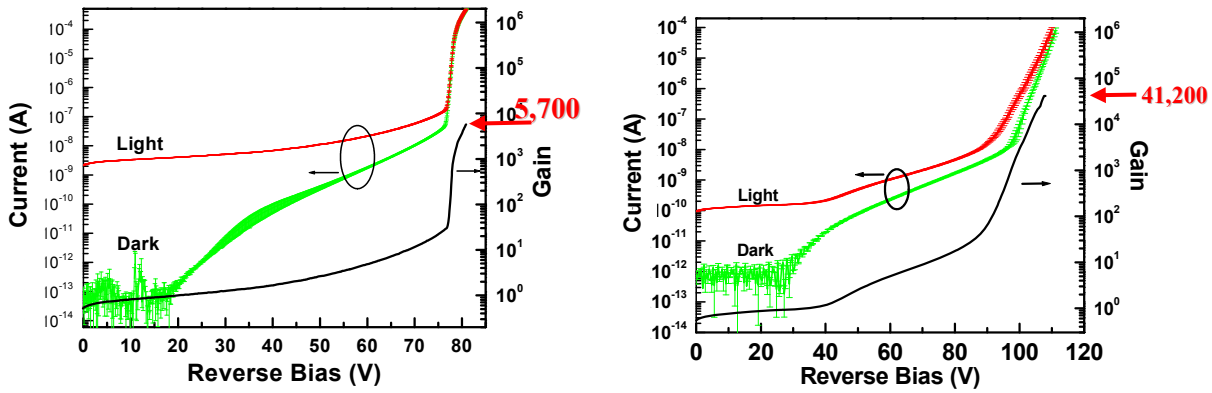

Figure 3. Left) Conventional *p*-*i*-*n* APD IV curves and gain. Right) SAM-APD IV curves and gain. In both plots, the left axis shows the measured dark and illuminated currents and the right axis shows the calculated gain.

The current remains fairly flat between zero and the reach-through voltage (V_{rt} = 40 V), and then begins to increase with larger reverse bias. To calculate the multiplication gain, we normalized the photocurrent, i.e. difference between light and dark currents, by the difference between the primary un-multiplied current and the un-multiplied dark current. The right axis of Figure 3 shows that the gain increases gradually from V_{rt}. Near the breakdown voltage, the avalanche

multiplication gain raises sharply up to a maximum value of 41,200 at 108 V. This represents a significant improvement from our best *p-i-n* APD's maximum gain of 5,700.

The spectral response was measured under back-illumination. At low voltages, the devices present a sharp response at around 364 nm, corresponding to the absorption edge of GaN; the response outside of this peak remains below the background noise of the set-up. This is believed to result from photons are absorbed close to the AlN interface. At the reach-through-voltage of 40 V the depletion region is fully extended, and a peak responsivity of 102.5 mA/W is achieved at 364 nm, corresponding to an external quantum efficiency of greater than 35 %. In addition, the optical response at shorter wavelengths becomes evident in the spectrum.

In conclusion, the performance of back-illuminated GaN APDs with separate absorption and multiplication regions has been demonstrated and their performance analyzed. In the SAM-APD, higher gain and lower noise than in regular *p-i-n* diodes were achieved through the enhancement of the hole-initiated multiplication.

4. P-TYPE DELTA DOPING FOR IMPROVED APD PERFORMANCE

A number of groups have recently been working to improving *p*-type GaN through the development and optimization of δ-doping.[28,29,30] In δ-doping the doping profile is implemented as follows: 1) a specific thickness of GaN is deposited normally to grow the GaN period, 2) the TMGa flow is then stopped and the crystal surface is allowed to nitridize, and finally 3) a DCpMg flow is introduced for a specific Mg flow time. The dopant flow is then stopped and TMGa resumed so that the cycle can repeat as the next GaN period is grown.[13] This is in contrast to conventional bulk *p*-type doping samples, TMGa and DCpMg are supplied together. A schematic diagram of the delta doping scheme is shown below in Figure 4.

4.1 Delta doping Optimization

Before growing SAM-APDs with δ-doped p-GaN regions, a series of calibration growths were performed to help optimize the δ-doping sequence. A 250 nm layer of *p*-GaN is grown either via conventional bulk growth, or delta-doping on the same 600-nm-thick AlN/LT-AlN buffer/sapphire template used to realize back-illuminated APDs.

The GaN period was initially fixed at 10 nm. The nitridation time was then varied from 15 to 120 seconds; however no significant changes in the hole concentration were observed. Thus, an intermediate nitridation time of 30s was chosen to ensure a stable GaN surface before the Mg flow is introduced. The Mg flow time was then varied from 15 to 60s. With increasing Mg flow time the hole concentration increases and mobility decreases. However for intermediate times the higher hole concentration compensates the mobility decrease leading to a reduction in resistivity with increasing Mg flow time. Comparing the δ-doping with intermediate Mg flow time to the conventional doping, around two orders of magnitude higher doping is achieved by δ-doping under the same growth conditions, with four times lower resistivity. This led us to chose an optimum Mg flow time of 60s. The last experiment was then to vary the GaN period. It was seen that with either larger or smaller periods than the initial 10 nm, the resistivity increases and the hole concentration decreases. For more details on delta doping optimization see ref. 30.

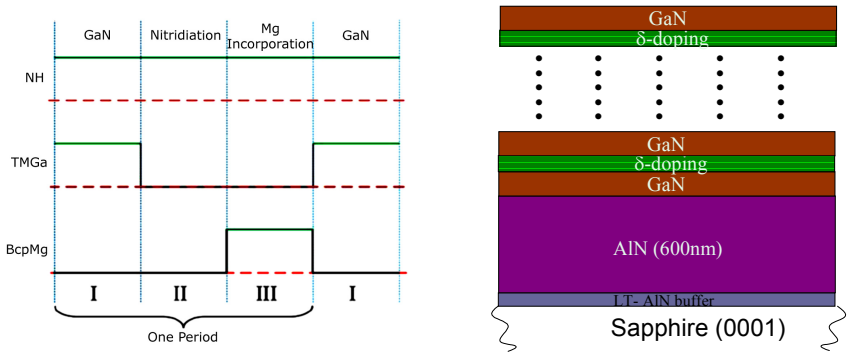

Figure 4. Left) δ-doping precursor profile showing the three step delta doping sequence. Right) Cross-sectional diagram of the δ-doped *p*-GaN test structures used to calibrate the δ-doping.[30]

After full optimization, the delta-doping structure is 10 nm of GaN followed by a 30 second nitridation and doped through a 60 s Mg flow time. This results in a *p*-type carrier concentration of 9.4×10^{17} cm^{-3}. A conventionally grown bulk doped structure grown under the same conditions had a significantly lower carrier concentration. However it is possible to obtain carrier concentration in the high 10^{17} or low 10^{18} region by decreasing the growth temperature or increasing the growth pressure.[13] However structural characterization of these layers reveals that the quality of the δ-doped *p*-GaN is significantly higher.

4.2 Delta-doped SAM-APDs

The optimized delta doping is then applied to the growth of SAM APDs to investigate the influence of the *p*-GaN quality on the device performance. For comparison a device was also grown using the same growth conditions, but conventionally doping the *p*-GaN layer. The SAM APD structure and processing are the same as discussed in Section 3. After processing, the current-voltage (*I-V*) characteristics under reverse bias were measured in darkness and under illumination, using a Xe lamp filtered at 360 nm using a band-pass filter (optical power = 11 nW). The light and dark I-V curves are measured alternatively three times in a row to ensure consistent device operation. The resulting measured I-V curves for both devices are shown below in Figure 5 along with the calculated gains. At reach through the δ-doped sample present an average dark current that is a factor of four lower than the dark current obtained in bulk doped sample. This reduction shows the important role the *p*-GaN layer plays in the origin of the leakage current and confirms the superior quality of the δ-doped samples.

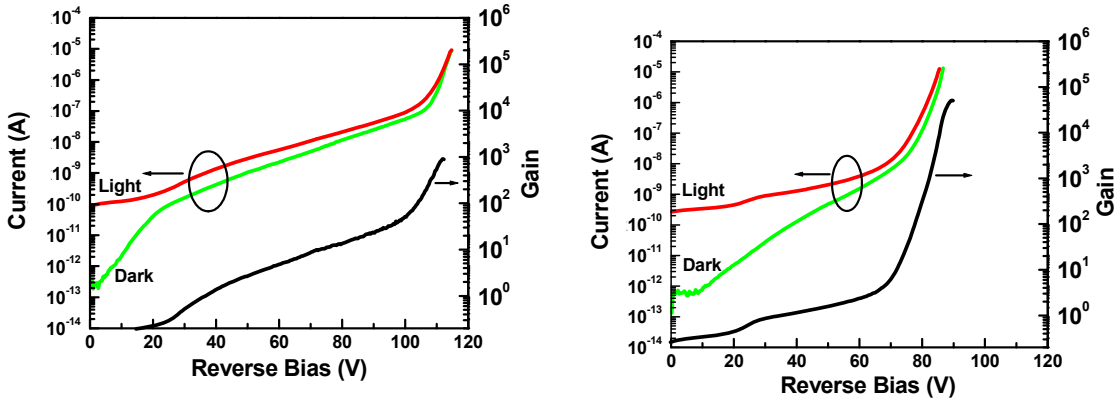

Figure 5. Both devices were grown under identical growth conditions. Left) shows the I-V curves and gain of the conventional bulk p-GaN SAM-APD. Right) Shows the IV curves and gain of the delta-doped SAM-APD. In both plots, the left axis shows the measured dark and illuminated currents and the right axis shows the calculated gain.

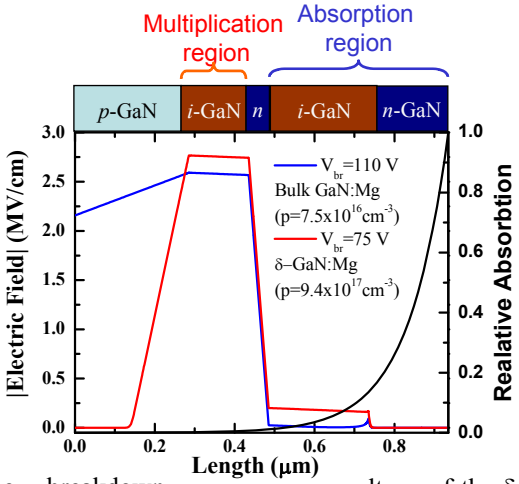

Figure 6. Simulated 1D electric field profiles of the δ-doped (red) and conventional bulk-doped (blue) SAM-APDs devices both biased at their breakdown voltages (V_{BR}).

The breakdown voltage of the δ-doped SAM-APD is 75 V whereas that of the bulk-doped is 110 V. The difference in breakdown voltage is primarily due to the better confinement of the electric field related to the higher

p-doping afforded by the δ-doped *p*-GaN. A 1-D finite element simulation of the electric field is shown above in

Figure 6. Based on this calculation the average electric field in the multiplication region at the onset of breakdown is 2.7 MV/cm in the δ-doped SAM-APD and 2.6 MV/cm in the bulk-doped SAM-APD: both of these are close to their theoretical value.[8] In the delta doped device, after breakdown, the avalanche multiplication reaches a maximum value of 51,000. This is more than 50 times higher than that of the bulk-doped device grown under the same conditions (left of Figure 5). The improvement of the *p*-GaN quality even enables higher gains than the smaller area SAM APD discussed in Section 3 that was grown with optimized conventional bulk *p*-GaN doping, thus emphasizing the importance of the high quality δ-doped *p*-layer.

In conclusion, high quality δ-doped *p*-GaN has been used to realize ultraviolet back-illuminated SAM-APDs. The higher quality of the δ-doped *p*-GaN results in lower leakage currents, a lower breakdown voltage, and a higher maximum gain compared to bulk-doped SAM-APD devices.

5. INTERSUBBAND SAMPLES MATERIAL GROWTH AND PROCESSING

The material was grown in an AIXTRON 200/4-HT horizontal flow low-pressure MOCVD reactor. Double-side polished (001) sapphire was used as the substrate. Growth on the sapphire substrate was nucleated with a thin 200 Å low-temperature AlN buffer layer. On top of this a 600-nm thick high quality AlN template layer[31] was grown by atomic layer epitaxy at a temperature of ~1300°C.

In order to realize intersubband structures, Trimethlyaluminum (TMAl), trimethylgallium (TMGa), and trimethlyindium (TMIn) are the metal-organic cation precursors for Al, Ga, and In, respectively; hydrogen is used as the carrier gas. Ammonia (NH_3) with a flow rate of 1.9 lt/min was used as the nitrogen source. TMGa and TMAl flow rate were 63.8 μmol/min and 48.8 μmol/min, respectively. Silane (SiH_4) is used as the n-type dopant source. All intersubband structure growth is performed at a pressure of 50 mbar and a temperature of 1035 ºC. SLs were grown with different thicknesses. None of the SL samples grown in this study were observed to be cracked.

5.1 Overview of Pulsed Growth Technique

AlN/GaN SL, despite the lattice mismatch of 2.4%, can be realized crack-free and be grown pseudomorphically.[32] However III-Nitrides are piezoelectric materials, in conventional c-plane growth; these highly strained layers generate multi-MV/cm electric fields.[33] Thus, interface or SL thickness fluctuations degrade the absorption quality significantly.[33] Another problem is AlN/GaN or GaN/AlN interface stability, and their dependence on (GaN or AlN) template.[34, 35] Moreover, the embedded GaN layer gets thinner during subsequent AlN growth.[36,37] All these observations necessitate further MOCVD growth studies. To overcome the limitations of MOCVD growth, we propose and analyze a novel pulsed deposition technique for realizing AlN/GaN SLs, and demonstrate ISB absorption at telecommunication wavelengths.

Using conventional MOCVD growth, parasitic pre-reactions [38] between the TMAl and NH_3 necessitate lower pressures and smaller V/III ratios. The lack of aluminum adatom mobility also urges higher growth temperatures for AlN growth. In contrast, GaN typically obtains higher quality when grown under higher pressures and larger V/III ratios with moderate temperatures. The challenge in realizing high-quality SLs for ISB transitions is to find growth conditions that work simultaneously for both of these materials and yield well defined interfaces. One way to deposit GaN with a high V/III ratio while decreasing the parasitic pre-reactions when depositing AlN, is to use temporal separation of TMAl and NH_3 (or pulsing). This enhances the surface adatom migration of both the GaN and AlN and maximizes the growth efficiency.[39]

The proposed SL deposition technique has two stages AlN grows, and GaN growth which each consist of two different steps for a total of four different steps as shown in

Figure 7: Steps (I) and (II) result in AlN deposition, and may be repeated several times to obtain thicker AlN layers. The separate introduction of the group III and V precursors into the growth chamber in an alternating sequence enhances the diffusion length of aluminum adatoms leading to higher quality material. Step (III) deposits GaN using conventional bulk deposition to ensure a high V/III ratio. Step (IV) nitridizes the surface before aluminum deposition for the next SL period. This step prepares the surface for AlN regrowth by eliminating the excess gallium on the interface that may otherwise form an AlGaN interlayer, thus degrading the interface sharpness. Thicker GaN layers may be realized by either varying the length of the bulk-like growth step (Step (III)) or by repeating steps (III) and (IV). By using this pulsed SL deposition technique, the V/III ratio for AlN is decreased whereas that of GaN is maximized. This allows for a much higher AlN growth rate and aluminum adatom mobility than would be achieved with conventional growth . A typical sketch of the SL is given in the inset of Figure 8(a).

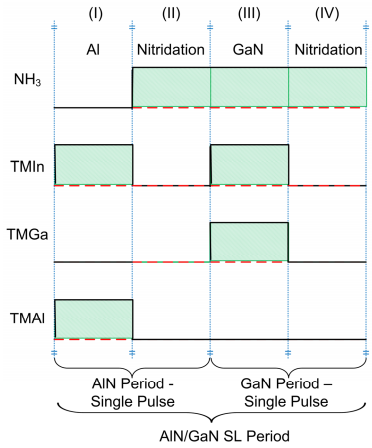

Figure 7: The growth sequence of AlN/GaN SL. One period consists of two main deposition phases: (1) AlN deposition, which is realized via pulsing TMAl and NH_3 to enhance aluminum adatom mobility (steps (I) and (II)), and (2) conventional GaN deposition (step (III)), which is realized by conventionally supplying TMGa and NH_3 simultaneously. Step IV nitridizes the surface.

5.2 Tunability of AlN and GaN Layers in the SL

Tunability of the well (GaN) and barrier (AlN) thickness are studied by growing AlN/GaN SL (as in Figure 8(a) inset) via varying the number of AlN pulses (steps (I) and steps (II)), GaN pulses (Steps (III) and (IV)) or the amount of GaN deposition time (for a single GaN pulse). XRD is used to characterize the SL. The angular separation between satellite peaks are used to calculate the SL period.[40] The average aluminum composition was calculated via $x_{Al} = \left(C_{AlGaN} - C^0_{GaN}\right) / \left(C^0_{AlN} - C^0_{GaN}\right)$ where C^0_{GaN} and C^0_{AlN} are the free-standing lattice parameters of GaN and AlN, and C_{AlGaN} is the average lattice constant of the SL determined from X-ray analysis.[40]

Fifty periods of various SL samples are grown, and layer thicknesses are deducted. The Figure 8(a) displays the AlN thickness dependency on number of AlN pulses. Similarly, GaN thickness dependency on GaN pulses and GaN deposition time are plotted in Figure 8(b) and (c), respectively. AlN (or GaN) thickness was found to be a linear function of AlN (or GaN) pulses. However, the linear fit to GaN thickness (Figure 8(b)(c)) intersect ordinate below abscissa which is attributed to the thinning of the GaN wells at high temperatures while AlN is being deposited.[36] Consequently, for the linear fit to AlN thickness (Figure 8(a)), the intersection with ordinate is above abscissa. However, a linear deposition growth rate with respect to AlN (or GaN) pulses and GaN deposition time is determined that makes this technique feasible for controllable AlN/GaN SL.

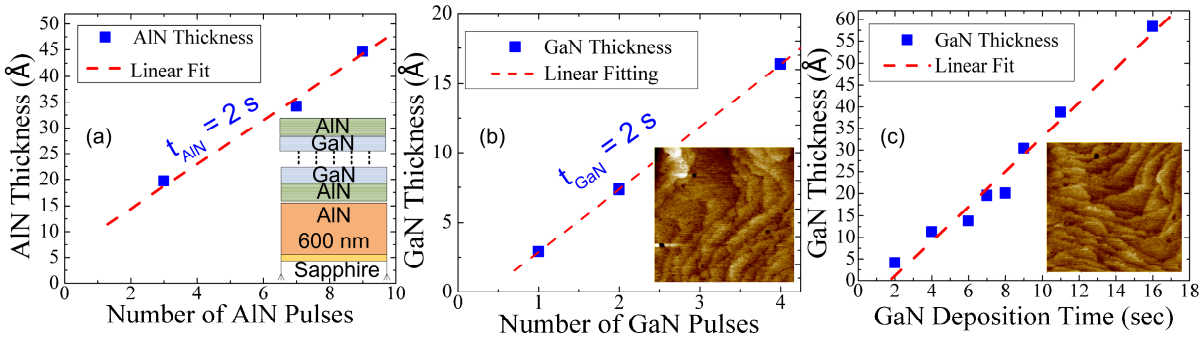

Figure 8: (a) AlN thickness versus number of AlN pulses for TMAl duration of 2 sec. Inset shows a cross-sectional diagram of a SL. (b) GaN thickness versus number of GaN pulses for TMGa duration of 2 sec. Inset shows the (1μm × 1μm) AFM SL surface without TMIn, (c) GaN thickness versus TMGa duration for a single GaN pulse. Inset shows the (1μm × 1μm) AFM SL surface with TMIn

Realizing different ISB devices requires tunability of the individual well (GaN) layer for a constant barrier (AlN) thickness. Keeping the AlN barrier thickness at 3.1±0.2 nm, we have varied the GaN thickness as 0.8, 2.6 and 3.5±0.2 nm via changing the GaN deposition time from 4, 9, and 11 seconds, respectively. XRD was employed to evaluate GaN and AlN thicknesses of the SLs. Fine satellite peaks were observed.[23]

5.3 Effect of Doping on Optical and Structural Quality

Doping the well *n*-type is realized via the introduction of SiH_4 along with the metalorganic cation sources (Steps (I) and (III)). SLs with the same amount of dopants either in the barrier- or well- are grown and no significant structural differences were observed by XRD or AFM.

In order to study the effect of doping on ISB absorption and assess the SL quality grown by our technique, we have grown 50 periods of {1.9 nm GaN with 3.1 nm AlN} SL on 600 nm AlN/c-sapphire with well doping levels of non-intentionally-doped ~10^{16}, slightly-doped 10^{17}, and highly doped 10^{19} cm^{-3}. Figure 9 below shows the (002) XRD Omega/2Theta scan for the SLs with different doping levels. No significant structural degradation with well-doping is observed.

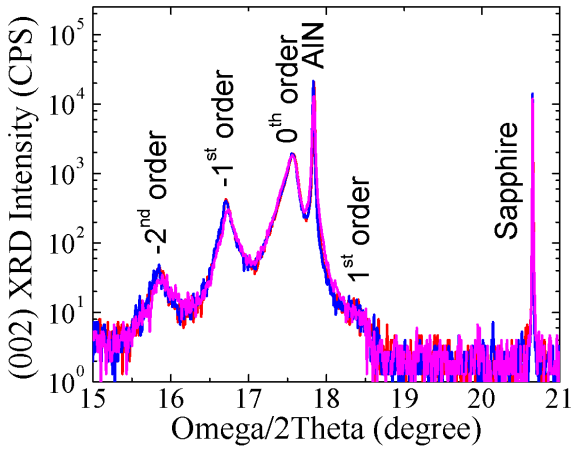

Figure 9 : (002) Omega/2Theta XRD of 50 period of {1.9 nm-thick GaN with 3.1-nm thick AlN} for different well n-doping levels.

5.4 Effect of Capping on the Optical and Structural Quality

The capping of the SL (50 periods of {1.8 nm-thick GaN / 3.1-nm thick AlN}) has been studied via photoluminescence (PL). Room temperature PL measurements are realized via frequency doubled Argon-Ion laser at 244 nm.
Figure 10 shows the PL spectra of uncapped, 30, and 100 nm (AlN) capped SLs whereas inset shows the XRD (002) omega/2Theta scans.

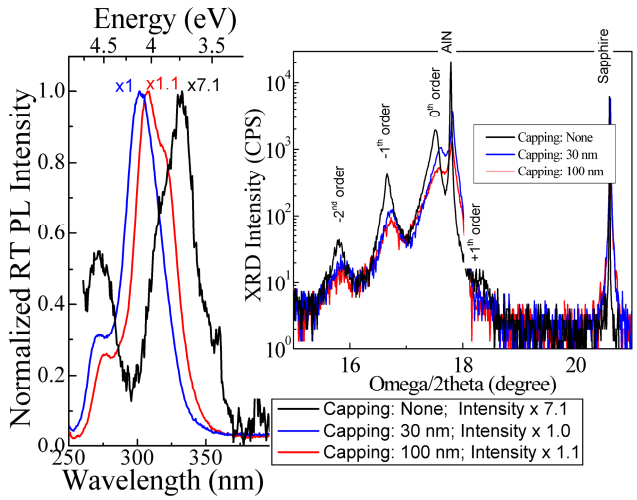

Figure 10: Room temperature PL of 50 period {1.8 nm-thick GaN / 3.1 nm-thick AlN} SL with different AlN capping thicknesses (uncapped, 30, and 100 nm). Inset shows (002) omega/2theta XRD of the SL with the different capping thicknesses.

Uncapped SLs are crack-free whereas few edge cracks are observed for the 30 nm capping, and become more prominent for the 100 nm capping (not shown). Thus, the significant blue shift observed with increasing capping is attributed to partial strain relief via crack-formation. Consequently, XRD satellite peaks are better defined for (crack-free) uncapped sample with respect to (cracked) capped ones. With the crack-formation, no significant period change is observed, however, the 0th order peak of SL moved towards the AlN template peak – an indicator of strain relief occurring. The PL intensity increases for capped SLs, which we attribute to the partial doping effect via band-bending due to the AlN capping layer.[41]

6. INTERSUBBAND ABSORPTION AND DISCUSSION

Samples were prepared for ISB absorption measurements by dicing to allow transverse optical access to the layers. Broad-band light from a blackbody source, either p- or s- polarized, was incident perpendicular to one side facet of the samples, traveled along the SL region and went out from the other facet. The infrared transmission was measured at room temperature using a Fourier transform infrared spectrometer (FTIR). The difference between the absorption of p- and s-polarized light was used to identify the ISB absorption.

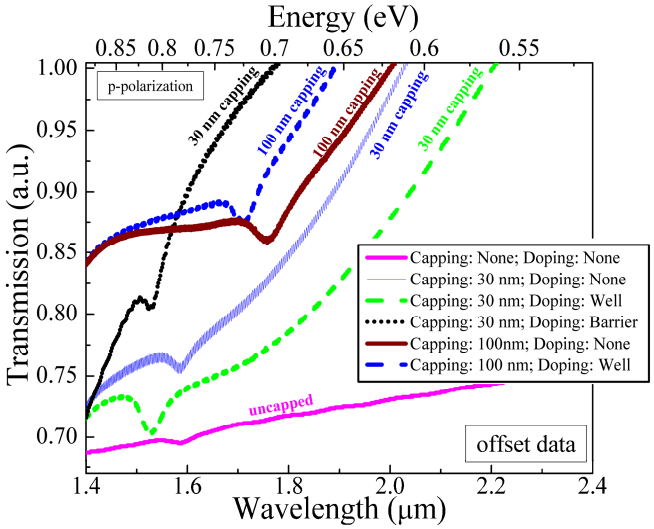

Figure 11: Relative (p-polarization) transmission of undoped, well- or barrier-doped, and uncapped, 30 or 100 nm capped 50 period {1.8 nm-thick GaN / 3.1-nm thick AlN} SL.

Figure 11displays the transmission of the p-polarized light for uncapped, 30, and 100 nm capped SLs, as well as undoped, well-doped , or barrier-doped samples. For uncapped samples, a weak absorption is observed. With 30 nm capping, the absorption is significantly increased. This is attributed to the unintentional doping generated by band bending with AlN capping,[41] and supports the increase in PL intensity observed. With thicker capping (100 nm), the absorption increased further. However, the strain relaxation via cracking is believed to lower the ISB transition energy

causing a red-shift (***Figure 11***). Irrespective of *n*-doping in barrier or well, ISB transition energy increased (blueshifted) with the addition of doping, due to many-body effects.[41] In conclusion, ISB absorption as low as 1.53 μm - the lowest wavelength reported by MOCVD - is realized and this technique is shown to be appropriate for near-infrared intersubband absorption.

7. CONCLUSION

In summary, back-illuminated separate absorption and multiplication APDs have been demonstrated. The pure hole injection of a back illuminated SAM-APD resulted in a gain as high as 41,000. By replacing the conventionally doped p-GaN with a novel high-quality δ-doped p-GaN layer the dark current could be reduced and the break down voltage lowered. This resulted in a maximum gain of 51,000.

A novel pulsing technique has been developed to realize high-quality superlattices by MOCVD that successfully demonstrated intersubband absorption at 1.53 μm. This has proved MOCVD as a reliable deposition technique for Nitride ISB devices. Doping is shown to blueshift the ISBTs. Besides, strain-relief via crack-formation is observed to red-shift the ISBTs. The correlation between material growth & characterization and theoretical predictions are studied. In summary, high quality GaN/AlN SLs are realized demonstrating the strong capabilities of MOCVD as a promising deposition technique for THz.

ACKNOWLEDGEMENTS

The authors would like to thank Dr. D. Silversmith of the AFOSR, Dr. H. Temkin and Dr. M. Rosker of DARPA, Dr. J. Zavada of ARO, and Dr. D. Cardimona of AFRL for discussions and encouragement.

REFERENCES

[1]. M. Razeghi, "Short-wavelength solar-blind detectors- status, prospects, and markets", Proc. IEEE, vol. **90**, pp. 1006-1014, (2002).

[2] C. Bayram, J. L. Pau, R. McClintock, and M. Razeghi, "Comprehensive study of blue and green multi-quantum-well light emitting diodes grown on conventional and lateral epitaxial overgrowth GaN," Applied Physics B 95, 307 (2009).

[3].P. Kung, A Yasan, R. McClintock, S.R. Darvish, K. Mi, M. Razeghi, "Future of AlxGa1-xN materials and device technology for ultraviolet photodetectors", Proc. SPIE, vol. **4650**, pp.199-206, (2002).

[4]. Hamamatsu Photonics, K.K., http://usa.hamamatsu.com/, PMTs based upon Cs-Te photocathodes such as R1080.

[5]. DARPA BAA06-14, Deep Ultraviolet Avalanche Photodetectors (DUVAP), (2005)

[6] C. Bayram, J. L. Pau, R. McClintock, M. Razeghi, M. P. Ulmer, and D. Silversmith, "High Quantum Efficiency Back-illuminated GaN Avalanche Photodiodes," Applied Physics Letters, vol. **93**, 211107 (2008).

[7] . C. Bayram, J. L. Pau, R. McClintock, and M. Razeghi, "Performance enhancement of GaN ultraviolet avalanche photodiodes with p-type delta-doping,"Applied Physics Letters, vol. **92**, 241103 (2008).

[8]. R. McClintock, J. L. Pau, K. Minder, C. Bayram, P. Kung, M. Razeghi, "Hole-initiated multiplication in back-illuminated GaN avalanche photodiodes," Applied Physics Letters 90, 1411121 (2007).

[9]. I.J. Oguzman, E. Bellotti, K. Brennan, J. Kolnik, R. Wang, and P. Ruden, "Theory of hole initiated impact ionization in bulk zincblende and wurtzite GaN", J. Appl. Phys. **81**, 7827 (1997).

[10]. X. Guo, L. B. Rowland, G. T. Dunne, J. A. Fronheiser, P. M. Sandvik, A. L. Beck, and J. C. Campbell, IEEE Photon Technology Letters, **18**,pp. 136 (2006).

[11]. J. C. Carrano, D. J. H. Lambert, C. J. Eiting, C. J. Collins, T. Li, S. Wang, B. Yang, A. L. Beck, R. D. Dupuis, and J. C. Campbell. Applied Physics Letters **76**, pp. 924 (2000).

[12]. P. Kozodoy, S. Keller, S.P. DenBaars, and U. K. Mishra, Journal of Crystal Growth **195**, 265 (1998).

[13]. C. Bayram, J. L. Pau, R. McClintock, and M. Razeghi, "Performance enhancement of GaN ultraviolet avalanche photodiodes with p-type delta-doping," Applied Physics Letters **92**(24) pp. 241103-1 (2008).

[14] L. Nevou, M. Tchernycheva, F.H. Julien, F. Guillot, and E. Monroy, 'Short wavelength (λ=2.13 μm) intersubband luminescence from GaN/AlN quantum wells at room temperature', Appl. Phys. Lett. 90, 121106 (2007).

[15] G. Sun, R. A. Sorel, 'Design and simulation of a GaN/AlGaN quantum cascade laser for terahertz emission' Microelectronics Journal 36, 450-452 (2005).

[16] N. Vukmirovic, V.D. Jovanovic, D. Indjin, Z. Ikonic, and P. Harrison, 'Optically pumped terahertz laser based on intersubband transitions in a GaN/AlGaN double quantum well', J. Appl. Phys. 97, 103106 (2005).
[17] K.Kishino, A. Kikuchi, H. Kanazawa, and T. Tachibana, "Intersubband transition in $(GaN)_m/(AlN)_n$ superlattices in the wavelength range from 1.08 to 1.61 μm", Appl. Phys. Lett. 81, 1234-1236 (2002).
[18] A. Helman, M. Tchernycheva, A. Lusson, E. Warde, F.H. Julien, Kh. Moumanis, G. Fishman, E. Monroy, B. Daudin, D. Le Si Dang, E. Bellet-Amalric, and D. Jalabert, 'Intersubband spectroscopy of doped and undoped GaN/AlN quantum wells grown by molecular-beam epitaxy' Appl. Phys. Lett. 83, 5196-5198 (2003).
[19] S. Nicolay, E. Feltin, J. –F Carlin, M. Mosca, L. Nevou, M. Tchernycheva, F. H. Julien, M. Ilegems, and N. Granjean, 'Indium surfactant effect on AlN/GaN heterostrcutures grown by metalor-organic vapor-phase epitaxy: Applications for intersubband transitions' Appl. Phys. Lett. 88, 151902 (2006).
[20] F. Guillot, E. Bellet-Amalric, E. Monroy, M.Tchernycheva, L. Nevou, L. Doyennette, F. H. Julien, Le Si Dang, T. Remmele, M. Albrecht, T. Shibata, and M. Tanaka, 'Si-doped GaN/AlN quantum dot superlattices for optoelectronics at telecommunication wavelengths' J. Appl. Phys. 100, 044326 (2006).
[21] G. Cywinski, C. Skierbiszewski, A. Fedunieiwcz-Zmuda, M. Siekacz, L. Nevou, L. Doyennette, M. Tchernycheva, F. H. Julien, P. Prystawko, M. Krysko, S. Grzanka, I. Grzegory, A. Presz, J.Z. Domagala, J. Smalc, M. Albrecht, T. Remmele, and S. Porowski, 'Growth of thin AlInN/GaInN quantum wells for applications to high-speed intersubband devices at telecommunication wavelengths' J. Vac. Sci. Technol. B 24(3) May/Jun (2006).
[22] E. Baumann, F.R. Giorgetta, D. Hofstetter, S. Golka, W. Scherenk, G. Strasser, L. Kirste, S. Nicolay, E. Feltin, J.F. Carlin, and N. Grandjean, 'Near Infrared absorption and room temperature photovoltaic response in AlN/GaN superlattices grown by metal-organic vapor-phase epitaxy' Appl. Phys. Lett. 89, 041106 (2006).
[23] C. Bayram, B. Fain, N. Péré-Laperne, R. McClintock, and M. Razeghi, "Pulsed metalorganic chemical vapor deposition of high quality AlN/GaN superlattices for intersubband transitions," Proc. SPIE 7222, 722212 (2009).
[24] C. Bayram, N. Péré-laperne, R. McClintock, B. Fain and M. Razeghi, "Pulsed Metalorganic Chemical Vapor Deposition of High Quality AlN/GaN Superlattices for Near-Infrared Intersubband Transitions," Applied Physics Letters, Vol 94, 121902 (2009).
[25]. J. F. Muth, J. D. Brown, M. A. L. Johnson, Z. Yu, R. M. Kolbas, J. W. Cook, Jr., and J. F. Schetzina, MRS Internet J. of Nitride Semicond. Res., **4S1**, 1 (1999).
[26]. E. Monroy, F. Calle, J. L. Pau, F. J. Sanchez, E. Munoz, F. Omnes, B. Beaumont, and P. Gibart, Journal of Applied Physics **88**, 2081 (2000).
[27]. K. A. McIntosh, R. J. Molnar, L. J. Mahoney, A. Lightfoot, M. W. Geis, K. M. Molvar, I. MeIngailis, R. L. Aggarwal, W. D. Goodhue, S. S. Choi, D. L. Spears, and S. Verghese, Appl. Phys. Lett. 75, 3485 (1999).
[28]. M.L. Nakarmi, K.H. Kim, J. Li, J.Y. Lin, and H.X. Jiang, Applied Physics Letters **82**, 3041 (2003).
[29]. C. Simbrunner, M. Wegscheider, M. Quast, Tian Li, A. Navarro-Quezada, H. Sitter, and A. Bonanni, Applied Physics Letters **90**, 142108 (2007).
[30]. C. Bayram, J.L. Pau, R. McClintock and M. Razeghi, "Delta-doping optimization for high quality p-type GaN," Journal of Applied Physics **104**(8) pp.083512 (2008).
[31] P. Kung, R. McClintock, J. L. P. Vizcaino, K. Minder, C. Bayram, and M. Razeghi, "III-nitride avalanche photodiodes," Proc. SPIE 6479, 64791J (2007).
[32] A.D. Bykhovski, B. L. Gelmont, and M.S. Shur, *J. Appl. Phys.* **81**, 6332 (1997).
[33] N. Suzuki, N. Iizuka, and K. Kaneko, *Jpn. J. Appl. Phys.* **42,** 132 (2002).
[34] C. Adelmann, E. Sarigiannidou, D. Jalabert, Y. Hori, J. –L. Rouviere, B. Daudin, S. Fanget, C. Bru-Chevallier, T. Shibata, and M. Tanaka, *Appl. Phys. Lett.* **82**, 4154 (2003).
[35] P. Boguslawski, K. Rapcewicz, and J.J. Bernholc, *Phys. Rev. B* **61** 10820 (2000).
[36] N. Gogneau, D. Jalabert, E. Monroy, E. Sarigiannidou, J.L. Rouviere, T. Shibata, M. Tanaka, J.M. Gerard, and B. Daudin, *J. Appl. Phys.* **96**, 1104 (2004).
[37] S. Nicolay, E. Feltin, J. –F. Carlin, N. Grandjean, L. Nevou, F.H. Julien, M. Schmidbauer, T. Remmele, and M. Albrecht, *Appl. Phys. Lett.* **91**, 061927 (2007).
[38] C. H. Chen, H. Liu, D. Steigerwald, W. Imler, C.P. Kuo, and M.G. Craford, *J. of Electron. Mater.* **25**, 1004 (1996).
[39] H.J. Kim, S. Choi, D. Yoo, J. –H. Ryou, R.S. Dupuis, R.F. Dalmau, P. Lu, and Z. Sitar, *Appl. Phys. Lett.* **93**, 022103 (2008).
[40] S. Zhou, M.F. Wu, S.D. Yao, B.S. Zhang, and H. Yang, *Superlattices and Microstructures* **40**, 137 (2006).

[41] P.K. Kandaswamy, F. Guillot, E. Bellet-Amalric, E. Monroy, L. Nevou, M. Tchernycheva, A. Michon, F.H. Julien, E. Baumann, F.R. Giorgetta, D. Hofstetter, T. Remmele, M. Albrecht, S. Birner, and Le Si Dang, *J.Appl. Phys.* **104**, 093501 (2008).